

MDPI

Article

Insight into the Binding of Argon to Cyclic Water Clusters from Symmetry-Adapted Perturbation Theory

Carly A. Rock and Gregory S. Tschumper *

Department of Chemistry and Biochemistry, University of Mississippi, University, MS 38677-1848, USA * Correspondence: tschumpr@olemiss.edu

Abstract: This work systematically examines the interactions between a single argon atom and the edges and faces of cyclic H_2O clusters containing three–five water molecules $(Ar(H_2O)_{n=3-5})$. Full geometry optimizations and subsequent harmonic vibrational frequency computations were performed using MP2 with a triple- ζ correlation consistent basis set augmented with diffuse functions on the heavy atoms (cc-pVTZ for H and aug-cc-pVTZ for O and Ar; denoted as haTZ). Optimized structures and harmonic vibrational frequencies were also obtained with the two-body-many-body (2b:Mb) and three-body-many-body (3b:Mb) techniques; here, high-level CCSD(T) computations capture up through the two-body or three-body contributions from the many-body expansion, respectively, while less demanding MP2 computations recover all higher-order contributions. Five unique stationary points have been identified in which Ar binds to the cyclic water trimer, along with four for (H₂O)₄ and three for (H₂O)₅. To the best of our knowledge, eleven of these twelve structures have been characterized here for the first time. Ar consistently binds more strongly to the faces than the edges of the cyclic $(H_2O)_n$ clusters, by as much as a factor of two. The 3b:Mb electronic energies computed with the haTZ basis set indicate that Ar binds to the faces of the water clusters by at least 3 kJ mol $^{-1}$ and by nearly 6 kJ mol $^{-1}$ for one Ar(H₂O)₅ complex. An analysis of the interaction energies for the different binding motifs based on symmetry-adapted perturbation theory (SAPT) indicates that dispersion interactions are primarily responsible for the observed trends. The binding of a single Ar atom to a face of these cyclic water clusters can induce perturbations to the harmonic vibrational frequencies on the order of 5 cm⁻¹ for some hydrogen-bonded OH stretching frequencies.

Keywords: water clusters; argon tagging; vibrational frequencies; interaction energies; binding energies



Citation: Rock, C.A.; Tschumper, G.S. Insight into the Binding of Argon to Cyclic Water Clusters from Symmetry-Adapted Perturbation Theory. *Int. J. Mol. Sci.* 2023, 24, 17480. https://doi.org/10.3390/ijms242417480

Academic Editor: M. Natália D.S. Cordeiro

Received: 29 November 2023 Revised: 6 December 2023 Accepted: 7 December 2023 Published: 14 December 2023



Copyright: © 2023 by the authors. Licensee MDPI, Basel, Switzerland. This article is an open access article distributed under the terms and conditions of the Creative Commons Attribution (CC BY) license (https://creativecommons.org/licenses/by/4.0/).

1. Introduction

Noble gases are frequently used as carrier gases and as inert environments in a broad range of spectroscopic techniques. Supersonic expansions [1–12], cryogenic matrices [13–35], and helium nanodroplets [36–42] are specific examples that continue to play important roles in the experimental characterization of weakly bound molecular complexes. Spectroscopic studies of neutral hydrogen-bonded clusters, including H_2O clusters, sometimes utilize one or more noble gas atoms (typically Ar) as an experimental tag to probe structural features, enhance experimental signals and even examine the hydrophobic effect [43–71].

Although the noble gases are inert under these types of experimental conditions, they can still perturb the molecules and complexes being studied [3,7,31,51,55,72–77]. Several studies involving Ar-tagged complexes demonstrate the potential of Ar to engage in favorable intermolecular dispersion and induction interactions when utilized as an isotropic probe of electron density to provide insight into regions of a molecule or molecular cluster of interest [51,53,54,58,59,62–65,68,78].

The interaction between an Ar atom and a single H_2O molecule has been studied in great detail [69,79–93], but relatively few studies have looked at the interactions of Ar with the water dimer [69,87,94] or larger water clusters [95,96]. The present study systematically identifies the energetically favorable binding sites of a single Ar atom to the well-

characterized structures of cyclic $(H_2O)_{n=3-5}$ clusters [6,10,24,30,31,37,42,97-136] while also tracking structural and vibrational perturbations that occur. Symmetry-adapted perturbation theory is used to analyze the interaction energies for the different binding motifs.

2. Computational Details

The lowest-energy binding sites of a single Ar atom around small water clusters with three–five water molecules $(Ar(H_2O)_{n=3-5})$ were identified via full geometry optimizations and harmonic vibrational frequency computations using MP2 [137] and Dunning's correlation-consistent cc-pVTZ [138] basis set for H atoms and aug-cc-pVTZ [139,140] for the "heavy atoms" (O and Ar), hereafter denoted as haTZ. A subsequent set of haTZ geometry optimizations and harmonic vibrational frequency computations were performed on the MP2/haTZ-identified stationary points with the highly efficient and accurate Nbody-many-body (Nb:Mb) technique [134,141-143] that captures all leading dominant N-body contributions to the many-body expansion (MBE) of the interactions in a cluster using an accurate high-level method, whereas the remaining higher-order contributions are recovered with a less demanding low-level method. For this study, we have selected the 2b:Mb [142–147] and 3b:Mb [141,143] versions of the Nb:Mb procedure. In this implementation, CCSD(T) [148] is used as the high-level method to describe the one- and two-body terms in the MBE of the cluster energy for 2b:Mb (as well as the three-body interactions for 3b:Mb) while MP2 is used as the low-level method to recover the higher-order \geq threebody contributions to the MBE (or \geq 4-body for 3b:Mb) by means of a computation on the entire cluster. Analytic gradients were used for all geometry optimizations along with analytic Hessians for all harmonic vibrational frequency computations. MP2 computations were carried out using Gaussian16 while all CCSD(T) computations were performed with CFOUR [149,150].

The relative electronic energies (ΔE) of the various complexes were calculated by comparing the total energies at each level of theory. The supramolecular approach was used to determine the MP2, 2b:Mb, and 3b:Mb binding energies (E_{bind}) and interaction energies (E_{int}) of the Ar atom to various water cluster isomers as shown in Equation (1).

$$E_{bind/int} = E[Ar(H_2O)_n] - E[(H_2O)_n] - E[Ar]$$
 (1)

 E_{bind} is obtained when $E[({\rm H_2O})_n]$ is evaluated using the fully optimized geometry of the isolated water cluster, whereas use of the geometry adopted in the full complex yields E_{int} . The effects of the harmonic zero-point vibrational energy (ZPVE) were also assessed for all minima, and the ZPVE-inclusive relative and binding energies are denoted ΔE^0 and E^0_{bind} respectively.

By comparing the total energy of a complex to the sum of fragment energies computed with finite basis sets, Equation (1) introduces an inconsistency commonly referred to as basis set superposition error (BSSE) [151,152]. To assess the potential effects of this inconsistency, the Boys–Bernardi counterpoise (CP) procedure [153,154] was employed to compute for the MP2/haTZ-optimized $Ar(H_2O)_{n=3-5}$ structures. This analysis utilized the protocol outlined elsewhere [155], which corresponds to the default CP scheme in Gaussian16, where the energies of the last two terms in Equation (1) are evaluated in the basis set of the entire cluster.

An additional analysis of the total interaction energies based on symmetry-adapted perturbation theory (SAPT) [156–158] was carried out on the 3b:Mb-optimized $Ar(H_2O)_{n=3-5}$ structures. We used the higher-order SAPT2+3(CCD) method that includes a treatment of dispersion based on coupled-cluster doubles and has been shown to provide improvements for challenging cases such as the PCCP dimer [159,160]. The SAPT2+3(CCD) computations were carried out with the haTZ basis set using the efficient implementation in the PSI4 [161,162] quantum chemistry software package that employs natural orbital truncation [163]. Rather than just calculating the total interaction energies as described above, SAPT provides additional insight into how Ar interacts with the small water clusters by

identifying the individual contributions from exchange repulsion, electrostatics, induction, and dispersion.

3. Results and Discussion

Twelve low-lying stationary points were identified for the $Ar(H_2O)_{n=3-5}$ systems via full geometry optimizations using the haTZ basis set in conjunction with the MP2, 2b:Mb, and 3b:Mb methods, and these structures are shown in Figure 1. Both the faces and edges of small, cyclic water clusters were identified as favorable binding sites for a single Ar atom. These H_2O stationary points include the well-characterized C_1 and C_3 trimers, S_4 , C_i and C_4 tetramers, and C_1 pentamer. The distance between the Ar atom and the corresponding face or edge binding site ranges from approximately 3.4 to 3.7 Å across the various $Ar(H_2O)_{n=3-5}$ binding motifs. Harmonic vibrational frequency computations confirm that these $Ar(H_2O)_{n=3-5}$ stationary points are minima at all levels of theory presented in this work. Cartesian coordinates and harmonic vibrational frequencies for all identified structures are reported in the Supporting Information (Tables S1–S36).

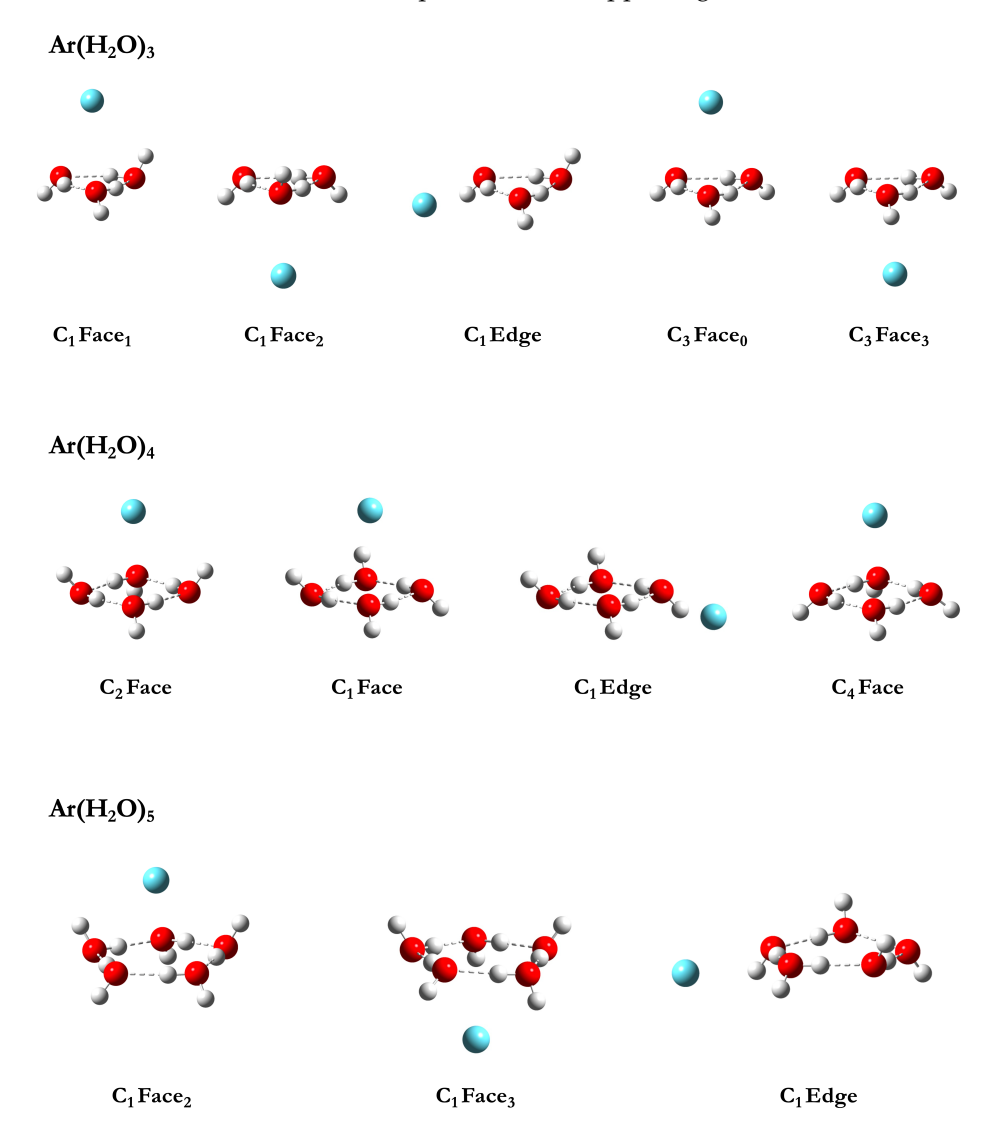


Figure 1. Minima identified for the $Ar(H_2O)_{n=3-5}$ complexes (H white; O red; Ar cyan).

The naming scheme shown in Figure 1 beneath each structure includes the point group symmetry of the $Ar(H_2O)_n$ cluster, the binding site of the Ar atom on the $(H_2O)_n$ cluster (face or edge) and the number of free hydrogens pointing towards the Ar atom when additional distinction is needed. For example, the first two structures listed at the top

Int. J. Mol. Sci. 2023, 24, 17480 4 of 15

left of Figure 1 for $Ar(H_2O)_3$ (C_1 Face₁ and C_1 Face₂, respectively) both have C_1 symmetry and Ar bound to the face of the water trimer. A subscript of 1 is added to the first structure name to indicate one free hydrogen pointing towards the Ar atom, while a subscript of 2 is added to the second structure name to indicate two free hydrogens pointing toward the Ar atom. This distinction is only necessary for some of the $Ar(H_2O)_3$ and $Ar(H_2O)_5$ clusters.

3.1. Structures, Harmonic Vibrational Frequencies, and Relative Energies

Table 1 reports the relative electronic and ZPVE-inclusive energies (ΔE and ΔE^0 , respectively) obtained with the haTZ basis set and the MP2, 2b:Mb, and 3b:Mb methods for all Ar(H₂O)_{n=3-5} minima depicted in Figure 1. The reference values of 0.00 kJ mol⁻¹ correspond to the lowest-energy structure for each Ar(H₂O)_n (n = 3, 4 and 5) cluster, each of which is depicted in the leftmost image of each row in Figure 1). The first five rows of Table 1 also include ΔE and ΔE^0 values for the bare C₁ and C₃ water trimers and S₄, C_i and C₄ water tetramers for reference. The haTZ relative electronic and ZPVE-inclusive energies reported in Table 1 are remarkably consistent between all three methods utilized in this work. The 2b:Mb values differ only slightly from the 3b:Mb results (average absolute deviation of 0.06 kJ mol⁻¹ and never by more than ±0.32 kJ mol⁻¹). The deviations from the 3b:Mb ΔE and ΔE^0 values tend to be slightly larger for the MP2 method, but they always fall within ±0.43 kJ mol⁻¹.

Table 1. Relative electronic and ZPVE-inclusive energies (ΔE and ΔE^0 , respectively) in kJ mol⁻¹ obtained for the haTZ-optimized (H₂O)_{n=3,4} and Ar(H₂O)_{n=3-5} structures using the MP2, 2b:Mb, and 3b:Mb methods.

Complex (H ₂ O) ₃ (H ₂ O) ₃	C ₁ C ₃ S ₄	ΔE 0.00 3.24 0.00	ΔE ⁰ 0.00 1.72	ΔE 0.00	ΔE^{0} 0.00	ΔE 0.00	ΔE^0
(H ₂ O) ₃	C_3 S_4	3.24			0.00	0.00	0.00
	S ₄		1.72			0.00	0.00
(II (0)		0.00		3.45	1.97	3.43	1.95
$(H_2O)_4$	Ċ	0.00	0.00	0.00	0.00	0.00	0.00
$(H_2O)_4$	C_i	3.88	2.96	3.92	3.00	3.91	2.98
$(H_2O)_4$	C_4^{\dagger}	9.11	a	9.34	a	9.31	a
$Ar(H_2O)_3$	C ₁ Face ₁	0.00	0.00	0.00	0.00	0.00	0.00
$Ar(H_2O)_3$	C ₁ Face ₂	0.36	0.23	0.27	0.17	0.27	0.17
$Ar(H_2O)_3$	C ₁ Edge	1.34	0.90	1.39	0.98	1.26	0.87
$Ar(H_2O)_3$	C ₃ Face ₀	3.10	1.75	3.40	2.00	3.37	1.98
$Ar(H_2O)_3$	C ₃ Face ₃	4.17	2.28	4.18	2.41	4.16	2.39
$Ar(H_2O)_4$	C ₂ Face ^b	0.00	0.00	0.00	0.00	0.00	0.00
$Ar(H_2O)_4$	C ₁ Face ^c	3.50	2.70	3.55	2.73	3.56	2.74
$Ar(H_2O)_4$	C ₁ Edge ^c	5.70	4.50	5.88	4.65	5.63	4.43
$Ar(H_2O)_4$	C ₄ Face	8.30	5.50	8.75	5.82	8.73	5.77
$Ar(H_2O)_5$	C ₁ Face ₂	0.00	0.00	0.00	0.00	0.00	0.00
$Ar(H_2O)_5$	C ₁ Face ₃	0.49	0.30	0.36	0.22	0.36	0.22
$Ar(H_2O)_5$	C ₁ Edge	2.90	2.44	3.03	2.58	2.71	2.31

 $^{^{}a}$ C_{4} † $(H_{2}O)_{4}$ is a transition state (harmonic vibrational frequencies in Supporting Information); b Ar bound to S_{4} $(H_{2}O)_{4}$; c Ar bound to C_{i} $(H_{2}O)_{4}$.

Note that ΔE^0 values are not provided for the C_4 bare $(H_2O)_4$ tetramer because it is a transition state (denoted by the superscript † symbol) with 1 imaginary vibrational frequency at all three levels of theory. The MP2, 2b:Mb, and 3b:Mb harmonic vibrational frequency computations with the haTZ basis set confirm that all of the other $(H_2O)_{n=3-5}$ and $Ar(H_2O)_{n=3-5}$ stationary points listed in Table 1 are minima. Shifts in the harmonic OH stretching frequencies induced by the binding of an Ar atom to a water trimer, tetramer, or pentamer $(Ar(H_2O)_{n=3-5})$ relative to the OH stretching frequencies of the isolated water cluster $((H_2O)_{n=3-5})$ were also analyzed. The formation of the $Ar(H_2O)_{n=3-5}$ complexes induces small shifts to lower energy (typically just 1 or 2 cm⁻¹) for every intramolecular

Int. J. Mol. Sci. 2023, 24, 17480 5 of 15

vibrational mode relative to the isolated water clusters. However, the shifts grow as large as -5 to -7 cm⁻¹ for some of the hydrogen-bonded OH stretching frequencies when a single Ar atom binds to the face of these cyclic $(H_2O)_{n=3-5}$ clusters. For comparison, the analogous experimental shifts induced by cryogenic Ar matrices and Ar nanocoatings range from approximately -15 to -35 cm⁻¹. (see Table II from Ref. [96]). The shifts predicted with the haTZ basis set are quite consistent across the MP2, 2b:Mb, and 3b:Mb CCSD(T):MP2 methods, and the harmonic vibrational frequencies are reported in the Supporting Information for all $Ar(H_2O)_{n=3-5}$ complexes identified in this work.

3.1.1. $Ar(H_2O)_3$

Five structures were identified as minima for the $Ar(H_2O)_3$ system in which Ar binds to either a face or an edge of the C_1 and C_3 water trimer isomers. All unique faces and edges were tested as potential binding sites for a single Ar atom, but the subsequent geometry optimizations always collapsed to one of the five structures reported here. The five binding motifs are shown in the first row of Figure 1; to the best of our knowledge, the rightmost C_3 Face₃ configuration is the only one that has been previously reported in the literature [95].

Ar binds to both unique faces of the C_1 water trimer, as well as the edge in which both free hydrogens are oriented in the same direction. Ar also binds to both unique faces of the C_3 water trimer, but does not bind to an edge. All five identified minima are separated by only a few kJ mol $^{-1}$ at all three levels of theory, as can be seen from the ΔE and ΔE^0 data near the middle of Table 1. The structure with the lowest energy has the single Ar on the face of the C_1 trimer with only one free hydrogen oriented towards the Ar atom (leftmost image in Figure 1). However, the structure with Ar bound to the other face (C_1 Face $_2$) is only higher in energy by a few tenths of a kJ mol $^{-1}$. The energy increases more significantly when Ar binds to an edge of the cyclic water trimer in the C_1 Edge structure, where ΔE grows to more than 1.2 kJ mol $^{-1}$. The C_3 Face $_0$ and C_3 Face $_3$ structures also have the largest relative energies, but this difference does not necessarily indicate weak binding (which will be discussed in greater detail in Section 3.2). It is almost entirely due to the underlying energy difference between the C_1 and C_3 isomers of the water trimer as shown in the first two rows of Table 1.

3.1.2. $Ar(H_2O)_4$

The second row of Figure 1 depicts the four minima identified for the $Ar(H_2O)_4$ system in which Ar binds to the S_4 , C_i and C_4 cyclic structures of $(H_2O)_4$. To the best of our knowledge, none of these complexes have been previously reported. The structure with the lowest energy has the Ar atom on the face of the S_4 global minimum of $(H_2O)_4$, which results in an $Ar(H_2O)_4$ complex with C_2 symmetry (leftmost image in the second row of Figure 1). No minima were identified with Ar binding to the edge of the S_4 water tetramer at the levels of theory used in this work. However, when Ar is in the presence of the C_i $(H_2O)_4$ structure, minima were identified with Ar bound not only to the face but also to the edge with both free hydrogens oriented in the same direction (analogous to the situation for the $Ar(H_2O)_3$ system). The resulting C_1 Face and C_1 Edge $Ar(H_2O)_4$ complexes have electronic energies higher than the C_2 Face minimum by at least 3.5 and 5.6 kJ mol $^{-1}$, respectively.

The highest-energy minimum identified (rightmost image in the second row of Figure 1) involves Ar binding to the face of the C_4 water tetramer structure with all free hydrogens on the opposite side of the ring, which gives an $Ar(H_2O)_4$ complex that maintains C_4 symmetry. Interestingly, the C_4 structure of the isolated $(H_2O)_4$ cluster is a transition state even though the corresponding complex with an Ar atom is a minimum at each level of theory reported here. Furthermore, scans of the Ar atom moving along the C_4 axis on the side of the ring with the four free H atoms yielded repulsive potential energy curves. As can be seen from the C_4 Face $Ar(H_2O)_4$ row of data in in Table 1, the 2b:Mb and 3b:Mb ΔE results grow beyond 8.7 kJ mol $^{-1}$. As noted for the water trimer systems, however, large ΔE and ΔE^0 values do not necessarily indicate weak interactions between

Int. J. Mol. Sci. 2023, 24, 17480 6 of 15

the Ar atom and the water cluster. (see Section 3.2). The large relative energies for C_4 Face $Ar(H_2O)_4$ primarily reflect that the C_4 transition state of $(H_2O)_4$ has an electronic energy approximately 9 kJ mol⁻¹ higher than the S_4 global minimum structure of the water tetramer (fifth row of data in Table 1).

3.1.3. $Ar(H_2O)_5$

The last row of Figure 1 shows the three $Ar(H_2O)_5$ minima identified with the MP2, 2b:Mb, and 3b:Mb methods in conjunction with the haTZ basis set. The two unique faces of the cyclic water pentamer provide similar binding sites for the Ar atom, but the electronic energy is slightly lower when it binds to the side with two free hydrogens (leftmost image in bottom row of Figure 1) rather than three (middle image in bottom row of Figure 1). The 3b:Mb ΔE for the latter $(Ar(H_2O)_5 \ C_1 \ Face_3)$ is only 0.36 kJ mol⁻¹. A minimum with Ar bound to an edge was also identified. As with the water trimer and tetramer clusters, a minimum for this motif was only found along the edge with both free hydrogens pointing to the same side of the $(H_2O)_n$ ring. To the best of our knowledge, all three binding motifs are reported here for the first time. The last row of Table 1 shows the C_1 Edge $Ar(H_2O)_5$ structure is noticeably higher in energy compared to the C_1 Face₂ minimum, with both ΔE and ΔE^0 growing larger than 2.3 kJ mol⁻¹. Binding sites on the cyclic C_5 $(H_2O)_5$ pentamer, analogous to those for the C_3 trimer and C_4 tetramer, were also investigated. However, all attempts to identify minima on the corresponding faces and edges collapsed to one of the C_1 structures shown in the bottom of row of Figure 1.

3.2. Binding and Interaction Energies

3.2.1. Binding Energies

The electronic and ZPVE-inclusive binding energies (E_{bind} and E_{bind}^0) of the haTZ optimized Ar(H₂O)_{n=3-5} minima are reported in Table 2 for the MP2, 2b:Mb, and 3b:Mb methods. Note that E_{bind}^0 values are not provided for the C₄ Ar(H₂O)₄ complex as the bare (H₂O)₄ tetramer fragment is a transition state at the associated levels of theory. All three methods are in remarkably good agreement for both quantities. The MP2 and 2b:Mb values (left and middle columns of Table 2) deviate by less than 0.3 kJ mol⁻¹ from the corresponding 3b:Mb E_{bind} and E_{bind}^0 data in the last two columns of Table 2. For comparison, the electronic binding energy of the ArH₂O dimer computed with the same procedures is approximately -1.2 kJ mol⁻¹.

Overall, the tabulated E_{bind} and E_{bind}^0 data show that Ar binds more strongly to the cyclic water clusters as the size increases from n=3 (top 3 rows of data in Table 2) to n=5 (bottom 3 rows of data in Table 2). Although the enhancement is quite modest when Ar binds to the edge of the cluster (less than 0.5 kJ mol^{-1}), the binding of Ar to a face of C_1 (H_2O)₅ is approximately 2 kJ mol⁻¹ stronger than to a face of C_1 (H_2O)₃. The 3b:Mb E_{bind} values in Table 2 clearly show that Ar binds more strongly to the faces of the water clusters than the edges, and due to the aforementioned trends, the energetic advantage of binding to a face becomes more pronounced as the cluster size increases (from 1.26 kJ mol⁻¹ (or 41%) for n=3 to 2.07 and 2.71 kJ mol⁻¹ (or 50% and 56%) for n=4 and 5). The C_1 Ar(H_2O)₅ Face₂ and Face₃ complexes exhibit the strongest binding energies out of all of the Ar(H_2O)_{n=3-5} minima identified in this work with E_{bind} exceeding -5.3 kJ mol^{-1} and approaching -5.8 kJ mol^{-1} . The electronic binding energies indicate that Ar binds slightly more strongly to faces that have fewer free hydrogens oriented towards the Ar atom (by approximately 0.3 kJ mol^{-1} for C_1 Face₁ vs. Face₂ Ar(H_2O)₃, 0.8 kJ mol^{-1} for C_3 Face₀ vs. Face₃ Ar(H_2O)₅, and 0.4 kJ mol^{-1} for C_1 Face₂ vs. Face₃ Ar(H_2O)₅).

When the CP procedure was employed to evaluate the potential impact of the BSSE on the binding energies for the $Ar(H_2O)_{n=3-5}$ minima identified in this work, the MP2/haTZ binding energies were found to decrease in magnitude by approximately 1.1 kJ mol⁻¹ on average and never by more than 1.5 kJ mol⁻¹ for all 12 configurations. These relatively small differences suggest that the results presented in Table 2 are only slightly larger in magnitude that the corresponding values evaluated at the complete basis set limit, where

Int. J. Mol. Sci. 2023, 24, 17480 7 of 15

by definition, the BSSE vanishes. All binding energies obtained with the CP procedure can be found in the Supporting Information (Tables S37–S39).

Table 2. Electronic and ZPVE-inclusive binding energies (E_{bind} and E_{bind}^0 , respectively) in kJ mol ⁻¹
for the haTZ-optimized $Ar(H_2O)_{n=3-5}$ complexes with the MP2, 2b:Mb, and 3b:Mb methods.

	MP2		2b:	Mb	3b:N	Иb		
Label	E_{bind}	E^0_{bind}	E_{bind}	E^0_{bind}	Ebind	E^0_{bind}		
Binding Process: C_1 (H_2O) ₃ + $Ar \rightarrow C_1$ $Ar(H_2O)_3$								
C ₁ Face ₁	-3.88	-3.10	-3.99	-3.21	-3.84	-3.09		
C ₁ Face ₂	-3.52	-2.87	-3.73	-3.04	-3.57	-2.92		
C ₁ Edge	-2.54	-2.20	-2.60	-2.23	-2.58	-2.23		
Binding Process: C_3 ($H_2O)_3 + Ar \rightarrow C_3$ Ar($H_2O)_3$								
C ₃ Face ₀	-4.02	-3.07	-4.04	-3.18	-3.90	-3.06		
C ₃ Face ₃	-2.95	-2.53	-3.26	-2.77	-3.11	-2.65		
Binding Process: S_4 (H_2O) ₄ + $Ar \rightarrow C_2$ $Ar(H_2O)_4$								
C ₂ Face	-4.65	-3.92	-4.84	-4.08	-4.62	-3.90		
Binding Process: C_i (H ₂ O) ₄ + Ar \rightarrow C ₁ Ar(H ₂ O) ₄								
C ₁ Face	-5.03	-4.18	-5.21	-4.34	-4.98	-4.16		
C ₁ Edge	-2.82	-2.39	-2.88	-2.42	-2.91	-2.46		
Binding Process: C_4^{\dagger} (H ₂ O) ₄ + Ar \rightarrow C ₄ Ar(H ₂ O) ₄								
C ₄ Face			-5.43		-5.20	a		
Binding Process: C_1 (H_2O) ₅ + $Ar \rightarrow C_1$ $Ar(H_2O)_5$								
C ₁ Face ₂	-5.85	-4.92	-6.03	-5.09	-5.75	-4.86		
C ₁ Face ₃	-5.36	-4.61	-5.67	-4.87	-5.39	-4.64		
C ₁ Edge	-2.95	-2.47	-3.01	-2.51	-3.04	-2.55		

^a C₄[†] (H₂O)₄ is a transition state (harmonic vibrational frequencies in Supporting Information).

3.2.2. Interaction Energies

The first three columns of Table 3 report the interaction energies (E_{int} in kJ mol⁻¹) calculated for the haTZ optimized Ar(H₂O)_{n=3-5} minima depicted in Figure 1 using the MP2, 2b:Mb and 3b:Mb methods, respectively. The remaining columns report the individual energy components of and the total interaction energy (in kJ mol⁻¹) obtained from SAPT2+3(CCD) computations with the haTZ basis set for the 3b:Mb/haTZ-optimized Ar(H₂O)_{n=3-5} minima. Utilizing SAPT to compute the total interaction energy directly provides the physical contributions from exchange repulsion, electrostatics, induction and dispersion, which are reported in the last four columns of Table 3, respectively.

The MP2, 2b:Mb, and 3b:Mb E_{int} values reported in the left half of Table 3 are in remarkably good agreement with the corresponding binding energies reported in Table 2, with differences never exceeding 0.14 kJ mol⁻¹ across all of the different structures examined and methods utilized in this study. The consistency between E_{int} and E_{bind} values suggest that the binding of an Ar atom to a cyclic water trimer, tetramer or pentamer does not induce any significant geometric changes to the $(H_2O)_n$ cluster itself. This observation is consistent with the small perturbations to the intramolecular vibrational frequencies that occur upon binding as noted in Section 3.1.

While the SAPT2+3(CCD) interaction energy values in Table 3 are somewhat smaller in magnitude than the MP2, 2b:Mb, and 3b:Mb E_{int} values, they are also slightly larger than the corresponding MP2 results obtained with the CP procedure that are tabulated in the Supporting Information (Tables S37–S39) which is to be expected because SAPT does not suffer from the BSSE issues introduced via Equation (1). All computations reveal stronger interactions for complexes in which Ar is bound to a face of the water cluster rather than an edge, and the SAPT analysis provides some insight into the underlying factors. The penultimate column of data in Table 3, for example, shows that induction consistently has the smallest contribution to E_{int} . Additionally, the attractive induction component is only slightly smaller in magnitude for the C_1 Edge structures than the analogous C_1 Face minima (by ca. 0.1 to 0.3 kJ mol⁻¹). The electrostatic contributions, which include short-range terms

from the overlap of the electron cloud of Ar with that of the water cluster, are larger than those from induction and also favor the face-binding motifs over the edge-binding ones by approximately 0.6 to 1.3 kJ mol $^{-1}$. In all cases, dispersion (last column of Table 3) is the dominant attractive contribution to E_{int} for these systems in which Ar binds to the edge or face of a cyclic water trimer, tetramer or pentamer. The dispersion components from the SAPT2+3(CCD) computations also exhibit the largest energetic differences between the C_1 Edge and corresponding C_1 Face structures, being more attractive in the latter by ca. 2 to 5 kJ mol $^{-1}$. Although all attractive contributions from the SAPT analysis (electrostatics, induction and dispersion) favor the face-binding motifs, the situation is reversed for exchange repulsion, which is smaller for the C_1 Edge structures than the corresponding C_1 Face motifs by approximately 2 to 4 kJ mol $^{-1}$. Nevertheless, the contributions from exchange repulsion are not enough to offset the attractive components, and the total SAPT2+3(CCD) E_{int} values are larger in magnitude for the lowest-energy C_1 Face minima of the Ar(H_2O) $_n$ clusters than the C_1 Edge structures by 1.09, 1.80 and 2.41 kJ mol $^{-1}$ for n = 3, 4, 5, respectively.

Table 3. Interaction energies (E_{int} in kJ mol⁻¹) calculated for the Ar(H₂O)_{n=3-5} minima using the MP2, 2b:Mb, and 3b:Mb methods with the haTZ basis set as well as the SAPT2+3(CCD) total interaction energies computed with the haTZ basis set for the 3b:Mb/haTZ optimized structures followed by the individual contributions from exchange repulsion, electrostatics, induction, and dispersion (in kJ mol⁻¹).

	E _{int}							
Label	MP2	2b:Mb	3b:Mb	SAPT	Exch	Elect	Ind	Disp
Binding Process: C_1 (H_2O) ₃ + $Ar \rightarrow C_1$ $Ar(H_2O)_3$								
C ₁ Face ₁	-3.90	-4.00	-3.85	-3.13	+5.62	-1.73	-0.66	-6.37
C ₁ Face ₂	-3.53	-3.74	-3.58	-2.92	+5.42	-1.71	-0.55	-6.08
C ₁ Edge	-2.54	-2.60	-2.58	-2.04	+3.66	-1.09	-0.40	-4.22
Binding Process: C_3 ($H_2O)_3 + Ar \rightarrow C_3$ Ar($H_2O)_3$								
C ₃ Face ₀	-4.03	-4.04	-3.90	-3.08	+5.41	-1.63	-0.53	-6.33
C ₃ Face ₃	-2.95	-3.26	-3.11	-2.43	+4.96	-1.60	-0.20	-5.59
Binding Process: S_4 ($H_2O)_4 + Ar \rightarrow C_2$ $Ar(H_2O)_4$								
C ₂ Face	-4.71	-4.90	-4.66	-3.71	+6.94	-2.17	-0.39	-8.08
Binding Process: C_i (H ₂ O) ₄ + Ar \rightarrow C ₁ Ar(H ₂ O) ₄								
C ₁ Face	-5.05	-5.23	-4.99	-4.08	+7.20	-2.23	-0.77	-8.28
C ₁ Edge	-2.83	-2.89	-2.91	-2.28	+4.05	-1.23	-0.44	-4.65
Binding Process: C_4^{\dagger} (H ₂ O) ₄ + Ar \rightarrow C_4 Ar(H ₂ O) ₄								
C ₄ Face	-5.48	-5.44°	-5.20	-4.09	+7.30	-2.16	-0.53	-8.69
Binding Process: C_1 ($H_2O)_5 + Ar \rightarrow C_1$ Ar($H_2O)_5$								
C ₁ Face ₂	-5.97	-6.15	-5.84	-4.79	+8.51	-2.64	-0.57	-10.01
C ₁ Face ₃	-5.50	-5.81	-5.50	-4.42	+8.29	-2.63	-0.45	-9.62
C ₁ Edge	-2.96	-3.01	-3.05	-2.38	+4.28	-1.31	-0.49	-4.86

4. Conclusions

This work systematically identifies the energetically favorable binding sites of a single Ar atom to the well-characterized structures of the cyclic $(H_2O)_{n=3-5}$ trimer, tetramer and pentamer clusters using the haTZ basis set and a variety of methods including MP2 and the highly efficient and accurate 2b:Mb and 3b:Mb methods. Twelve unique $Ar(H_2O)_{n=3-5}$ stationary points have been identified in which Ar binds to either a face or an edge on the water cluster via full geometry optimizations and have been confirmed as minima by harmonic vibrational frequency computations at all three levels of theory. Five, four and three unique stationary points have been identified in which Ar binds to the C_1 and C_3 water trimers, S_4 , C_i and C_4 water tetramers and C_1 water pentamer, respectively. To the best of our knowledge, all of these structures are characterized here for the first time with the exception of the C_3 Face₃ complex. [95]

Although multiple minima were identified with the Ar bound to a face of each water cluster (9 total), only a single minimum was identified for each value of n with Ar bound to an edge (3 total). In every case, a face provided a more energetically favorable binding

site for the Ar atom than an edge of the same $(H_2O)_n$ cluster. Relative electronic energies (with and without ZPVE correction) ranged from approximately 1 to 3 kJ mol⁻¹ higher in energy for the latter complexes. The binding energies $(E_{bind}$ and E_{bind}^0) also show that Ar consistently binds more strongly to the faces of the water clusters than the edges (by ca. 1 to 3 kJ mol⁻¹).

The MP2, 2b:Mb, and 3b:Mb electronic interaction energies (E_{int}) computed with the haTZ basis set are nearly identical to the corresponding E_{bind} values, suggesting that the binding of an Ar atom has no significant effect on the geometries of the bare (H_2O)_{n=3-5} clusters. The small differences between E_{bind} and E_{int} are also consistent with the very small changes to (nearly) all intramolecular harmonic vibrational frequencies of the water clusters after Ar binds to an edge or face. However, the frequency shifts can be on the order of -5 cm⁻¹ for some of the hydrogen-bonded OH stretching frequencies when a single Ar atom binds to a face of these small cyclic water clusters.

The haTZ total interaction energies computed with SAPT2+3(CCD) qualitatively support these findings, resulting in stronger interaction energies for complexes with Ar bound to a face rather than an edge, with the differences between the SAPT2+3(CCD) values exceeding 2 kJ mol⁻¹ between the two potential binding sites. Notably, using SAPT to compute the total interaction energy provides further insight into the nature of these favorable interactions between Ar and small cyclic water clusters by providing a breakdown of the total interaction energy into physically meaningful components (electrostatics, exchange repulsion, induction and dispersion).

SAPT2+3(CCD) computations with the haTZ basis set indicate that dispersion overwhelmingly provides the dominant attractive component to E_{int} in all cases. It also exhibited the greatest difference between the edge- and face-binding motifs, favoring the latter by just over 2 kJ mol⁻¹ for the trimer and growing to more than 5 kJ mol⁻¹ for the pentamer.

The results presented here for 2-dimensional hydrogen-bonded networks provide some guidelines for the expected binding patterns that Ar will exhibit in larger 3-dimensional water clusters. In the case of $(H_2O)_6$, for example, an Ar atom is expected to preferentially bind to the faces rather than the edges edges of the low-lying minima (prism, cage, etc.). Additionally, the interaction strength should increase with the size of the face (from triangular to rectangular and pentagonal), but the overall perturbations to the relative energetics and vibrational frequencies of the hexamer isomers will likely remain quite small and similar in magnitude to those reported here.

Supplementary Materials: The supporting information can be downloaded at: https://www.mdpi.com/article/10.3390/ijms242417480/s1.

Author Contributions: Conceptualization, methodology, and funding acquisition, G.S.T.; Investigation and data curation, C.A.R.; Writing—original draft, C.A.R.; Writing—review & editing, G.S.T. All authors have read and agreed to the published version of the manuscript.

Funding: This work is supported in part by the National Science Foundation (CHE-2154403).

Institutional Review Board Statement: Not applicable.

Informed Consent Statement: Not applicable.

Data Availability Statement: Data are contained within the article and Supplementary Materials.

Acknowledgments: The Mississippi Center for Supercomputing Research (MCSR) is thanked for a generous allocation of time on their computational resources.

Conflicts of Interest: The authors declare no conflict of interest.

References

- 1. Liu, K.; Brown, M.G.; Carter, C.; Saykally, R.J.; Gregory, J.K.; Clary, D.C. Characterization of a cage form of the water hexamer. *Nature* **1996**, *381*, 501–503. [CrossRef]
- 2. Liu, K.; Brown, M.G.; Saykally, R.J. Terahertz Laser Vibration-Rotation Tunneling Spectroscopy and Dipole Moment of a Cage Form of the Water Hexamer. *J. Phys. Chem. A* **1997**, *101*, 8995–9010. [CrossRef]

3. Klots, T.D.; Ruoff, R.S.; Gutowsky, H.S. Rotational spectrum and structure of the linear CO₂-HCN dimer: Dependence of isomer formation on carrier gas. *J. Chem. Phys.* **1989**, *90*, 4216–4221. [CrossRef]

- 4. Ruoff, R.S.; Klots, T.D.; Emilsson, T.; Gutowsky, H.S. Relaxation of conformers and isomers in seeded supersonic jets of inert gases. *J. Chem. Phys.* **1990**, *93*, 3142–3150. [CrossRef]
- 5. Emilsson, T.; Germann, T.C.; Gutowsky, H.S. Kinetics of molecular association and relaxation in a pulsed supersonic expansion. *J. Chem. Phys.* **1992**, *96*, 8830–8839. [CrossRef]
- 6. Steinbach, C.; Andersson, P.; Melzer, M.; Kazimirski, J.K.; Buck, U.; Buch, V. Detection of the book isomer from the OH-stretch spectroscopy of size selected water hexamers. *Phys. Chem. Chem. Phys.* **2004**, *6*, 3320–3324. [CrossRef]
- 7. Pérez, C.; Muckle, M.T.; Zaleski, D.P.; Seifert, N.A.; Temelso, B.; Shields, G.C.; Kisiel, Z.; Pate, B.H. Structures of Cage, Prism, and Book Isomers of Water Hexamer from Broadband Rotational Spectroscopy. *Science* **2012**, *336*, 897–901. [CrossRef] [PubMed]
- 8. Pérez, C.; Lobsiger, S.; Seifert, N.A.; Zaleski, D.P.; Temelso, B.; Shields, G.C.; Kisiel, Z.; Pate, B.H. Broadband Fourier transform rotational spectroscopy for structure determination: The water heptamer. *Chem. Phys. Lett.* **2013**, *571*, 1–15. [CrossRef]
- 9. Pérez, C.; Zaleski, D.P.; Seifert, N.A.; Temelso, B.; Shields, G.C.; Kisiel, Z.; Pate, B.H. Hydrogen Bond Cooperativity and the Three-Dimensional Structures of Water Nonamers and Decamers. *Angew. Chem.* **2014**, *53*, 14368–14372. [CrossRef]
- 10. Otto, K.E.; Xue, Z.; Zielke, P.; Suhm, M.A. The Raman spectrum of isolated water clusters. *Phys. Chem. Chem. Phys.* **2014**, 16, 9849–9858. [CrossRef]
- 11. Richardson, J.O.; Pérez, C.; Lobsiger, S.; Reid, A.A.; Temelso, B.; Shields, G.C.; Kisiel, Z.; Wales, D.J.; Pate, B.H.; Althorpe, S.C. Concerted hydrogen-bond breaking by quantum tunneling in the water hexamer prism. *Science* **2016**, *351*, 1310–1313. [CrossRef] [PubMed]
- 12. Cole, W.T.S.; Farrell, J.D.; Wales, D.J.; Saykally, R.J. Structure and torsional dynamics of the water octamer from THz laser spectroscopy near 215 μm. *Science* **2016**, 352, 1194–1197. [CrossRef]
- 13. Thiel, M.V.; Becker, E.D.; Pimentel, G.C. Infrared Studies of Hydrogen Bonding of Water by the Matrix Isolation Technique. *J. Chem. Phys.* **1957**, 27, 486–490. [CrossRef]
- 14. Redington, R.L.; Milligan, D.E. Infrared Spectroscopic Evidence for the Rotation of the Water Molecule in Solid Argon. *J. Chem. Phys.* **1962**, *37*, 2162–2166. [CrossRef]
- 15. Redington, R.L.; Milligan, D.E. Molecular Rotation and Ortho-Para Nuclear Spin Conversion of Water Suspended in Solid Ar, Kr and Xe. *J. Chem. Phys.* **1963**, *39*, 1276–1284. [CrossRef]
- 16. Ayers, G.P.; Pullin, A.D.E. The i.r. spectra of matrix isolated water species-I. Assignment of bands to (H₂O)₂, (D₂O)₂ and HDO dimer species in argon matrices. *Spectrochim. Acta Part A* **1976**, 32, 1629–1639. [CrossRef]
- 17. Bentwood, R.M.; Barnes, A.J.; Orvill-Thomas, W.J. Studies of intermolecular interactions by matrix isolation vibrational spectroscopy: Self-association of water. *J. Mol. Struct.* **1980**, *84*, 391–404. [CrossRef]
- 18. Engdahl, A.; Nelander, B. On the structure of the water trimer. A matrix isolation study. *J. Chem. Phys.* **1987**, *86*, 4831–4837. [CrossRef]
- 19. Knözinger, E.; Schuller, W.; Langel, W. Structure and dynamics in pure and doped rare-gas matrices. *Faraday Discuss. Chem. Soc.* **1988**, *86*, 285–293. [CrossRef]
- 20. Engdahl, A.; Nelander, B. Water in krypton matrices. J. Mol. Struct. 1989, 193, 101–109. [CrossRef]
- 21. Forney, D.; Jacox, M.E.; Thompson, W.E. The Mid- and Near-Infrared Spectra of Water and Water Dimer Isolated in Solid Neon. *J. Mol. Spectrosc.* **1993**, 157, 479–493. [CrossRef]
- 22. Perchard, J.P. Anharmonicity and hydrogen bonding. III. Analysis of the near infrared spectrum of water trapped in argon matrix. *Chem. Phys.* **2001**, 273, 217–233. [CrossRef]
- 23. Michaut, X.; Vasserot, A.M.; Abouaf-Marguin, L. Temperature and time effects on the rovibrational structure of fundamentals of H₂O trapped in solid argon: Hindered rotation and RTC satellite. *Vib. Spectrosc.* **2004**, *34*, 83–93. [CrossRef]
- 24. Ceponkus, J.; Karlström, G.; Nelander, B. Intermolecular Vibrations of the Water Trimer, a Matrix Isolation Study. *J. Phys. Chem. A* **2005**, *109*, 7859–7864. [CrossRef] [PubMed]
- 25. Hirabayashi, S.; Yamada, K.M.T. Infrared spectra of the H₂O-Kr and H₂O-Xe complexes in argon matrices. *Chem. Phys. Lett.* **2005**, 418, 323–327. [CrossRef]
- 26. Coussan, S.; Roubin, P.; Perchard, J.P. Infrared induced isomerizations of water polymers trapped in nitrogen matrix. *Chem. Phys.* **2006**, 324, 527–540. [CrossRef]
- 27. Abouaf-Marguin, L.; Vasserot, A.M.; Pardanaud, C.; Michaut, X. Nuclear spin conversion of water diluted in solid argon at 4.2 K: Environment and atmospheric impurities effects. *Chem. Phys. Lett.* **2007**, 447, 232–235. [CrossRef]
- 28. Pardanaud, C.; Vasserot, A.M.; Michaut, X.; Abouaf-Marguin, L. Observation of nuclear spin species conversion inside the 1593 cm⁻¹ structure of H₂O trapped in argon matrices: Nitrogen impurities and the H₂O:N₂ complex. *J. Mol. Struct.* **2008**, 873, 181–190. [CrossRef]
- 29. Ceponkus, J.; Uvdal, P.; Nelander, B. Acceptor switching and axial rotation of the water dimer in matrices, observed by infrared spectroscopy. *J. Chem. Phys.* **2010**, 133, 074301. [CrossRef]
- 30. Ceponkus, J.; Uvdal, P.; Nelander, B. Water Tetramer, Pentamer, and Hexamer in Inert Matrices. *J. Phys. Chem. A* 2012, 116, 4842–4850. [CrossRef]
- 31. Ceponkus, J.; Engdahl, A.; Uvdal, P.; Nelander, B. Structure and dynamics of small water clusters, trapped in inert matrices. *Chem. Phys. Lett.* **2013**, *581*, 1–9. [CrossRef]

32. Mukhopadhyay, A.; Cole, W.T.S.; Saykally, R.J. The water dimer I: Experimental characterization. *Chem. Phys. Lett.* **2015**, 633, 13–26. [CrossRef]

- 33. Pogorelov, V.Y.; Doroshenko, I.Y. Vibrational spectra of water clusters, trapped in low temperature matrices. *Low Temp. Phys.* **2016**, *42*, 1163–1166. [CrossRef]
- 34. Oswald, S.; Suhm, M.A.; Coussan, S. Incremental NH stretching downshift through stepwise nitrogen complexation of pyrrole: A combined jet expansion and matrix isolation study. *Phys. Chem. Chem. Phys.* **2019**, *21*, 1277. [CrossRef] [PubMed]
- 35. Oswald, S.; Coussan, S. Chloroform-nitrogen aggregates: Upshifted CH and downshifted CCl stretching vibrations observed by matrix isolation and jet expansion infrared spectroscopy. *Low Temp. Phys.* **2019**, *45*, 639–648. [CrossRef]
- Nauta, K.; Miller, R.E. Formation of Cyclic Water Hexamer in Liquid Helium: Smallest Piece of Ice. Science 2000, 287, 293–295.
 [CrossRef]
- 37. Burnham, C.J.; Xantheas, S.S.; Miller, M.A.; Applegate, B.E.; Miller, R.E. The formation of cyclic water complexes by sequential ring insertion: Experiment and theory. *J. Chem. Phys.* **2002**, *117*, 1109–1122. [CrossRef]
- 38. Lindsay, C.M.; Douberly, G.E.; Miller, R.E. Rotational and vibrational dynamics of H₂O and HDO in helium nanodroplets. *J. Mol. Struct.* **2006**, *786*, 96–104. [CrossRef]
- 39. Kuyanov-Prozument, K.; Choi, M.Y.; Vilesov, A.F. Spectrum and infrared intensities of OH-stretching bands of water dimers. *J. Chem. Phys.* **2010**, 132, 014304. [CrossRef] [PubMed]
- 40. Schwan, R.; Kaufmann, M.; Leicht, D.; Schwaab, G.; Havenith, M. Infrared spectroscopy of the ν_2 band of the water monomer and small water clusters (H₂O)_{n=2,3,4} in helium droplets. *Phys. Chem. Chem. Phys.* **2016**, *18*, 24063–24069. [CrossRef]
- 41. Douberly, G.E.; Miller, R.E.; Xantheas, S.S. Formation of Exotic Networks of Water Clusters in Helium Droplets Facilitated by the Presence of Neon Atoms. *J. Am. Chem. Soc.* **2017**, *139*, 4152–4156. [CrossRef] [PubMed]
- 42. Schwan, R.; Qu, C.; Mani, D.; Pal, N.; Schwaab, G.; Bowman, J.M.; Tschumper, G.S.; Havenith, M. Observation of the Low-Frequency Spectrum of the Water Trimer as a Sensitive Test of the Water-Trimer Potential and the Dipole-Moment Surface. *Angew. Chem.* **2020**, *59*, 11399–11407. [CrossRef] [PubMed]
- 43. Anderson, D.T.; Davis, S.; Nesbitt, D.J. Sequential solvation of HCl in argon: High resolution infrared spectroscopy of Ar_nHCl (n = 1, 2, 3). *J. Chem. Phys.* **1997**, 107, 1114–1127. [CrossRef]
- 44. Leung, H.O.; Gangwani, D.; Grabow, J.U. Nuclear Quadrupole Hyperfine Structure in the Microwave Spectrum of Ar-N₂O. *J. Mol. Spectrosc.* **1997**, *184*, 106–112. [CrossRef]
- 45. Häber, T. FTIR-Spectroscopy of isolated and argon coated (HBr) $_{n\leq 4}$ clusters in supersonic slit-jet expansions. *Phys. Chem. Chem. Phys.* **2003**, *5*, 1365–1369. [CrossRef]
- 46. Gregoire, G.; Brinkmann, N.R.; van Heijnsbergen, D.; Schaefer, H.F.; Duncan, M.A. Infrared Photodissociation Spectroscopy of Mg⁺(CO₂)_n and Mg⁺(CO₂)_nAr Clusters. *J. Phys. Chem. A* **2003**, 107, 218–227. [CrossRef]
- 47. Bochenkova, A.V.; Suhm, M.A.; Granovsky, A.A.; Nemukhin, A.V. Hybrid diatomics-in-molecules-based quantum mechanical/molecular mechanical approach applied to the modeling of structures and spectra of mixed molecular clusters $Ar_n(HCl)_m$ and $Ar_n(HF)_m$. *J. Chem. Phys.* **2004**, *120*, 3732–3743. [CrossRef]
- 48. Walker, N.R.; Walters, R.S.; Tsai, M.K.; Jordan, K.D.; Duncan, M.A. Infrared Photodissociation Spectroscopy of Mg⁺(H₂O)Ar_n Complexes: Isomers in Progressive Microsolvation. *J. Phys. Chem. A* **2005**, 109, 7057–7067. [CrossRef] [PubMed]
- 49. Douberly, G.E.; Walters, R.S.; Cui, J.; Jordan, K.D.; Duncan, M.A. Infrared Spectroscopy of Small Protonated Water Clusters, $H^+(H_2O)_n$ (n = 2-5): Isomers, Argon Tagging, and Deuteration. *J. Phys. Chem. A* **2010**, 114, 4570–4579. [CrossRef]
- 50. Carnegie, P.D.; Bandyopadhyay, B.; Duncan, M.A. Infrared Spectroscopy of Mn⁺(H₂O) and Mn²⁺(H₂O) via Argon Complex Predissociation. *J. Phys. Chem. A* **2011**, *115*, 7602–7609. [CrossRef]
- 51. Marshall, M.D.; Leung, H.O.; Calvert, C.E. Molecular structure of the argon-(Z)-1-chloro-2-fluoroethylene complex from chirped-pusle and narrow-band Fourier transform microwave spectroscopy. *J. Mol. Spectrosc.* **2012**, 280, 97–103. [CrossRef]
- 52. Fujii, A.; Mizuse, K. Infrared spectroscopic studies on hydrogen-bonded water networks in gas phase clusters. *Int. Rev. Phys. Chem.* **2013**, 32, 266–307. [CrossRef]
- 53. Leung, H.O.; Marshall, M.D.; Mueller, J.L.; Amberger, B.K. The molecular structure of and interconversion tunneling in the argon-cis-1,2-difluoroethylene complex. *J. Chem. Phys.* **2013**, *139*, 134303. [CrossRef]
- 54. Leung, H.O.; Marshall, M.D.; Messinger, J.P.; Knowlton, G.S.; Sundheim, K.M.; Cheung-Lau, J.C. The microwave spectra and molecular structures of 2-chloro-1,1-difluoroethylene and its complex with the argon atom. *J. Mol. Spectrosc.* **2014**, *305*, 25–33. [CrossRef]
- 55. Kaledin, M.; Adedeji, D.T. Driven Molecular Dynamics Studies of the Shared Proton Motion in the H₅O₂⁺·Ar Cluster: The Effect of Argon Tagging and Deuteration on Vibrational Spectra. *J. Phys. Chem. A* **2015**, *119*, 1875–1884. [CrossRef] [PubMed]
- 56. Li, J.W.; Morita, M.; Takahashi, K.; Kuo, J.L. Features in Vibrational Spectra Induced by Ar-Tagging for $H_3O^+Ar_m$, m = 0 3. J. Phys. Chem. A **2015**, 119, 10887–10892. [CrossRef] [PubMed]
- 57. Leung, H.O.; Marshall, M.D.; Wronkovich, M.A. The microwave spectrum and molecular structure of Ar-2,3,3,3-tetrafluoropropene. *J. Mol. Spectrosc.* **2017**, 337, 80–85. [CrossRef]
- 58. Marshall, M.D.; Leung, H.O. The microwave spectrum and molecular structure of 3,3-difluoro-1,2-epoxypropane and its complex with the argon atom. *J. Mol. Spectrosc.* **2018**, 350, 18–26. [CrossRef]

59. Marshall, M.D.; Leung, H.O.; Wang, K.; Acha, M.D. Microwave Spectrum and Molecular Structure of the Chiral Tagging Candidate, 3,3,3-Trifluoro-1,2-epoxypropane and Its Complex with the Argon Atom. *J. Phys. Chem. A* **2018**, 122, 4670–4680. [CrossRef] [PubMed]

- 60. Makarewicz, J.; Shirkov, L. Theoretical study of the complexes of dichlorobenzene isomers with argon. I. Global potential energy surface for all the isomers with application to intermolecular vibrations. *J. Chem. Phys.* **2019**, *150*, 074301. [CrossRef] [PubMed]
- 61. Shirkov, L.; Makarewicz, J. Theoretical study of the complexes of dichlorobenzene isomers with argon. II. SAPT analysis of the intermolecular interaction. *J. Chem. Phys.* **2019**, *150*, 074302. [CrossRef] [PubMed]
- 62. Marshall, M.D.; Leung, H.O.; Febles, O.; Gomez, A. The microwave spectra and molecular structures of (E)-1,3,3,3-tetrafluoropropene and its complex with the argon atom. *J. Mol. Spectrosc.* **2020**, *374*, 111379. [CrossRef]
- 63. Leung, H.O.; Marshall, M.D.; Stuart, D.J. Microwave Spectrum and Molecular Structure of 3-fluoro-1,2-epoxypropane and the Unexpected Structure of Its Complex with the Argon Atom. *J. Phys. Chem. A* **2020**, *124*, 1798–1810. [CrossRef] [PubMed]
- 64. Leung, H.O.; Marshall, M.D.; Horowitz, J.R.; Stuart, D.J. The microwave spectrum and molecular structure of the gas-phase heterodimer formed between argon and glycidol. *J. Mol. Spectrosc.* **2021**, *375*, 111407. [CrossRef]
- 65. Leung, H.O.; Marshall, M.D.; Bozzi, A.T.; Horowitz, J.R.; Nino, A.C.; Tandon, H.K.; Yoon, L. The microwave spectra and molecular structures of (E)-1-chloro-1,2-difluoroethylene and its complex with the argon atom. *J. Mol. Spectrosc.* **2021**, *381*, 111520. [CrossRef]
- 66. Punyain, W.; Takahashi, K. Evaluation of Ar tagging toward the vibrational spectra and zero point energy of X⁻HOH, X⁻DOH, and X⁻HOD, for X = F, Cl, Br. *Phys. Chem. Phys.* **2021**, 23, 9492–9499. [CrossRef] [PubMed]
- 67. Marks, J.H.; Miliordos, E.; Duncan, M.A. Infrared spectroscopy of RG-Co⁺(H₂O) complexes (RG = Ar, Ne, He): The role of rare gas "tag" atoms. *J. Chem. Phys.* **2021**, *154*, 064306. [CrossRef]
- 68. Leung, H.O.; Marshall, M.D.; Ahmad, T.Z.; Borden, D.W.; Hoffman, C.A.; Kim, N.A. The microwave spectra and molecular structures of the chiral and achiral rotamers of 2,3,3-trifluoropropene and their gas-phase heterodimers with the argon atom. *J. Mol. Spectrosc.* 2022, 387, 111656. [CrossRef]
- 69. Das, A.; Arunan, E. Measurement of Donor-Acceptor Interchange Tunnelling in Ar(H₂O)₂ using Rotational Spectroscopy and a Re-look at Its Structure and Bonding. *J. Mol. Struct.* **2022**, 1252, 132094. [CrossRef]
- 70. Ito, Y.; Kominato, M.; Nakashima, Y.; Ohshimo, K.; Misaizu, F. Fragment imaging in the infrared photodissociation of the Ar-tagged protonated water clusters H₃O⁺-Ar and H⁺(H₂O)₂-Ar. *Phys. Chem. Chem. Phys.* **2023**, 25, 9404–9412. [CrossRef]
- 71. Leung, H.O.; Marshall, M.D.; Hong, S.; Hoque, L. The microwave spectra and molecular structures of (Z)-1-chloro-3,3,3-trifluoropropene and its gas-phase heterodimer with the argon atom. *J. Mol. Spectrosc.* **2023**, *394*, 111779. [CrossRef]
- 72. Wassermann, T.N.; Luckhaus, D.; Coussan, S.; Suhm, M.A. Proton tunneling estimates for malonaldehyde vibrations from supersonic jet and matrix quenching experiments. *Phys. Chem. Chem. Phys.* **2006**, *8*, 2344–2348. [CrossRef] [PubMed]
- 73. Wassermann, T.N.; Zielke, P.; Lee, J.J.; Cezard, C.; Suhm, M.A. Structural preferences, argon nanocoating, and dimerization of *n*-alkanols as revealed by OH stretching spectroscopy in supersonic jets. *J. Phys. Chem. A* **2007**, *111*, 7437–7448. [CrossRef] [PubMed]
- 74. Wassermann, T.N.; Suhm, M.A. Ethanol monomers and dimers revisisted: A raman study of conformational preferences and argon nanocoating effects. *J. Phys. Chem. A* **2010**, *114*, 8223–8233. [CrossRef] [PubMed]
- 75. Lee, J.J.; Hofener, S.; Klopper, W.; Wassermann, T.N.; Suhm, M.A. Origin of the argon nanocoating shift in the OH stretching fundamental of n-propanol: A combined experimental and quantum chemical study. *J. Phys. Chem. C* **2009**, *113*, 10929–10938. [CrossRef]
- 76. Vasylieva, A.; Doroshenko, I.; Doroshenko, O.; Pogorelov, V. Effect of argon environment on small water clusters in matrix isolation. *Low Temp. Phys.* **2019**, *45*, 627–633. [CrossRef]
- 77. Vasylieva, A.; Doroshenko, I.; Stepanian, S.; Adamowicz, L. The influence of low-temperature argon matrix on embedded water clusters. A DFT theoretical study. *Low Temp. Phys.* **2021**, 47, 242–249. [CrossRef]
- 78. Kisiel, Z.; Fowler, P.W.; Legon, A.C. Rotational spectra and structures of van der Waals dimers of Ar with a series of fluorocarbons. *J. Chem. Phys.* **1991**, *95*, 2283–2291. [CrossRef]
- 79. Cohen, R.C.; Busarow, K.L.; Laughlin, K.B.; Blake, G.A.; Havenith, M.; Lee, Y.T.; Saykally, R.J. Tunable far infrared laser spectroscopy of van der Waals bonds: Vibration-rotation-tunneling spectra of Ar-H₂O. *J. Chem. Phys.* **1988**, *89*, 4494–4504. [CrossRef]
- 80. Cohen, R.C.; Busarow, K.L.; Lee, Y.Y.; Saykally, R.J. Tunable far infrared laser spectroscopy of van der Waals bonds: The intermolecular stretching vibration and effective radial potentials for Ar-H₂O. *J. Chem. Phys.* **1990**, 92, 169–177. [CrossRef]
- 81. Fraser, G.T.; Lovas, F.J.; Suenram, R.D.; Matsumura, K. Microwave spectrum of Ar-H₂O: Dipole moment, isotopic studies, and ¹⁷O quadrupole coupling constants. *J. Mol. Spectrosc.* **1990**, *144*, 97–112. [CrossRef]
- 82. Chałasiński, G.; Szczęśniak, M.M.; Scheiner, S. *Ab initio* study of the intermolecular potential of Ar-H₂O. *J. Chem. Phys.* **1991**, 94, 2807–2816. [CrossRef]
- 83. Cohen, R.C.; Saykally, R.J. Multidimensional intermolecular dynamics from tunable far-infrared laser spectroscopy: Angular-radial coupling in the intermolecular potential of argon-H₂O. *J. Chem. Phys.* **1991**, *95*, 7891–7906. [CrossRef]
- 84. Suzukí, S.; Bumgarner, R.E.; Stockman, P.A.; Green, P.G.; Blake, G.A. Tunable far-infrared laser spectroscopy of deuterated isotopomers of Ar-H₂O. *J. Chem. Phys.* **1991**, *94*, 824–825. [CrossRef]

85. Germann, T.C.; Gutowsky, H.S. Nuclear hyperfine interactions and dynamic state of H₂O in Ar-H₂O. *J. Chem. Phys.* **1993**, 98, 5235–5238. [CrossRef]

- 86. Tao, F.M.; Klemperer, W. Accurate ab initio potential energy surfaces of Ar-HF, Ar-H₂O, and Ar-NH₃. *J. Chem. Phys.* **1994**, 101, 1129–1145. [CrossRef]
- 87. Borges, E.; Ferreira, G.G.; Braga, J.P. Structures and energies of Ar_nH_2O (n = 1-26) clusters using a nonrigid potential surface: A molecular dynamics simulation. *Int. J. Quantum Chem.* **2008**, *108*, 2523–2529. [CrossRef]
- 88. Liu, X.; Xu, Y. New rovibrational bands of the Ar-H₂O complex at the ν_2 bend region of H₂O. *J. Mol. Spectrosc.* **2014**, 301, 1–8. [CrossRef]
- 89. Zou, L.; Weaver, S.L.W. Direct measurement of additional Ar-H₂O vibration-rotation-tunneling bands in the millimeter-submillimeter range. *J. Mol. Spectrosc.* **2016**, 324, 12–19. [CrossRef]
- 90. Hou, D.; Ma, Y.T.; Zhang, X.L.; Li, H. The origins of intra- and inter-molecular vibrational couplings: A case study of H₂O-Ar on full and reduced-dimensional potential energy surface. *J. Chem. Phys.* **2016**, 144, 014301. [CrossRef]
- 91. Vanfleteren, T.; Földes, T.; Herman, M.; Liévin, J.; Loreau, J.; Coudert, L.H. Experimental and theoretical investigations of H₂O-Ar. *J. Chem. Phys.* **2017**, 147, 014302. [CrossRef] [PubMed]
- 92. Yang, D.; Liu, L.; Xie, D.; Guo, H. Full-dimensional quantum studies of vibrational energy transfer dynamics between H₂O and Ar: Theory assessing experiment. *Phys. Chem. Chem. Phys.* **2022**, 24, 13542–13549. [CrossRef] [PubMed]
- 93. Liu, L.; Yang, D.; Guo, H.; Xie, D. Full-Dimensional Quantum Dynamics Studies of Ro-vibrationally Inelastic Scattering of H₂O with Ar: A Benchmark Test of the Rigid-Rotor Approximation. *J. Phys. Chem. A* **2023**, 127, 195–202. [CrossRef] [PubMed]
- 94. Arunan, E.; Emilsson, T.; Gutowsky, H.S. Rotational Spectra, Structure, and Dynamics of Ar_m - $(H_2O)_n$ Clusters: The Ar- $(H_2O)_2$ trimer. *J. Chem. Phys.* **2002**, *116*, 4886–4895. [CrossRef]
- 95. Arunan, E.; Emilsson, T.; Gutowsky, H.S. Rotational Spectra, Structure, and Dynamics of Ar_m - $(H_2O)_n$ Clusters: Ar_2 - H_2O , Ar_3 - H_2O , Ar- $(H_2O)_2$ and Ar- $(H_2O)_3$. *J. Am. Chem. Soc.* **1994**, *116*, 8418–8419. [CrossRef]
- 96. Moudens, A.; Georges, R.; Goubet, M.; Makarewicz, J.; Lokshtanov, S.E.; Vigasin, A.A. Direct absorption spectroscopy of water clusters formed in a continuous slit nozzle expansion. *J. Chem. Phys.* **2009**, *131*, 204312. [CrossRef] [PubMed]
- 97. Mó, O.; Yáñez, M.; Elguero, J. Cooperative (nonpairwise) effects in water trimers: An ab initio molecular orbital study. *J. Chem. Phys.* **1992**, *97*, 6628–6638. [CrossRef]
- 98. Pugliano, N.; Saykally, R.J. Measurement of Quantum Tunneling Between Chiral Isomers of the Cyclic Water Trimer. *Science* **1992**, 257, 1937–1940. [CrossRef]
- 99. Schütz, M.; Bürgi, T.; Leutwyler, S.; Bürgi, H.B. Fluxionality and low-lying transition structures of the water trimer. *J. Chem. Phys.* **1993**, 99, 5228–5238. [CrossRef]
- 100. Wales, D.J. Theoretical study of water trimer. J. Am. Chem. Soc. 1993, 115, 11180-11190. [CrossRef]
- 101. Xantheas, S.S.; Dunning, T.H. The structure of the water trimer from *abinitio* calculations. *J. Chem. Phys.* **1993**, *98*, 8037–8040. [CrossRef]
- 102. Xantheas, S.S.; Dunning, T.H. Ab *initio* studies of cyclic water clusters $(H_2O)_n$, n = 1-6. I. Optimal structures and vibrational spectra. *J. Chem. Phys.* **1993**, 99, 8774–8792. [CrossRef]
- 103. Xantheas, S.S. Ab *initio* studies of cyclic water clusters $(H_2O)_n$, n = 1-6. II. Analysis of many-body interactions. *J. Chem. Phys.* **1994**, 100, 7523–7534. [CrossRef]
- 104. Pribble, R.N.; Zwier, T.S. Size-Specific Infrared Spectra of Benzene- $(H_2O)_n$ Clusters (n = 1 through 7): Evidence for Noncyclic $(H_2O)_n$ Structures. *Science* **1994**, 265, 75–79. [CrossRef] [PubMed]
- 105. Liu, K.; Loeser, J.G.; Elrod, M.J.; Host, B.C.; Rzepiela, J.A.; Pugliano, N.; Saykally, R.J. Dynamics of Structural Rearrangements in the Water Trimer. *J. Am. Chem. Soc.* **1994**, *116*, 3507–3512. [CrossRef]
- 106. Xantheas, S.S. Ab *initio* studies of cyclic water clusters $(H_2O)_n$, n = 1-6. III. Comparison of density functional with MP2 results. *J. Chem. Phys.* **1995**, 102, 4505–4517. [CrossRef]
- 107. Schütz, M.; Klopper, W.; Lüthi, H.P.; Leutwyler, S. Low-lying stationary points and torsional interconversions of cyclic (H₂O)₄: An *abinitio* study. *J. Chem. Phys.* **1995**, *103*, 6114–6126. [CrossRef]
- 108. Fowler, J.E.; Schaefer, H.F.I. Detailed Study of the Water Trimer Potential Energy Surface. *J. Am. Chem. Soc.* **1995**, 117, 446–452. [CrossRef]
- 109. Wales, D.J.; Walsh, T.R. Theoretical study of the water pentamer. J. Chem. Phys. 1996, 105, 6957–6971. [CrossRef]
- 110. Huisken, F.; Kaloudis, M.; Kulcke, A. Infrared spectroscopy of small size-selected water clusters. *J. Chem. Phys.* **1996**, *104*, 17–25. [CrossRef]
- 111. Cruzan, J.D.; Braly, L.B.; Liu, K.; Brown, M.G.; Loeser, J.G.; Saykally, R.J. Quantifying Hydrogen Bond Cooperativity in Water: VRT Spectroscopy of the Water Tetramer. *Science* **1996**, *271*, 59–62. [CrossRef] [PubMed]
- 112. Liu, K.; Brown, M.G.; Cruzan, J.D.; Saykally, R.J. Vibration-Rotation Tunneling Spectra of the Water Pentamer: Structure and Dynamics. *Science* 1996, 271, 62–64. [CrossRef]
- 113. Paul, J.B.; Collier, C.P.; Saykally, R.J.; Scherer, J.J.; O'Keefe, A. Direct Measurement of Water Cluster Concentrations by Infrared Cavity Ringdown Laser Absorption Spectroscopy. *J. Phys. Chem. A* 1997, 101, 5211–5214. [CrossRef]
- 114. Wales, D.J.; Walsh, T.R. Theoretical study of the water tetramer. J. Chem. Phys. 1997, 106, 7193–7207. [CrossRef]
- 115. Nielsen, I.M.B.; Seidl, E.T.; Janssen, C.L. Accurate structures and binding energies for small water clusters: The water trimer. *J. Chem. Phys.* 1999, 110, 9435. [CrossRef]

116. Xantheas, S.S.; Burnham, C.J.; Harrison, R.J. Development of transferable interaction models for water. II. Accurate energetics of the first few water clusters from first principles. *J. Chem. Phys.* **2002**, *116*, 1493–1499. [CrossRef]

- 117. Taketsugu, T.; Wales, D.J. Theoretical study of rearrangements in water dimer and trimer. *Mol. Phys.* **2002**, *100*, 2793–2806. [CrossRef]
- 118. Anderson, J.A.; Crager, K.; Fedoroff, L.; Tschumper, G.S. Anchoring the potential energy surface of the cyclic water trimer. *J. Chem. Phys.* **2004**, *121*, 11023–11029. [CrossRef]
- 119. Day, M.B.; Kirschner, K.N.; Shields, G.C. Global Search for Minimum Energy (H₂O)_n Clusters, n = 3–5. *J. Phys. Chem. A* 2005, 109, 6773–6778. [CrossRef]
- 120. Dunn, M.E.; Evans, T.M.; Kirschner, K.N.; Shields, G.C. Prediction of Accurate Anharmonic Experimental Vibrational Frequencies for Water Clusters, $(H_2O)_n$, n = 2-5. *J. Phys. Chem. A* **2006**, *110*, 303–309. [CrossRef]
- 121. Slipchenko, M.N.; Kuyanov, K.E.; Sartakov, B.G.; Vilesov, A.F. Infrared intensity in small ammonia and water clusters. *J. Chem. Phys.* **2006**, 124, 241101. [CrossRef] [PubMed]
- 122. Hirabayashi, S.; Yamada, K.M.T. Infrared spectra and structure of water clusters trapped in argon and krypton matrices. *J. Mol. Struct.* **2006**, 795, 78–83. [CrossRef]
- 123. Hirabayashi, S.; Yamada, K.M.T. The monocyclic water hexamer detected in neon matrices by infrared spectroscopy. *Chem. Phys. Lett.* **2007**, 435, 74–78. [CrossRef]
- 124. Pérez, J.F.; Hadad, C.Z.; Restrepo, A. Structural Studies of the Water Tetramer. *Int. J. Quantum Chem.* **2008**, 108, 1653–1659. [CrossRef]
- 125. Watanabe, Y.; Maeda, S.; Ohno, K. Intramolecular vibrational frequencies of water clusters $(H_2O)_n$ (n = 2–5): Anharmonic analyses using potential functions based on the scaled hypersphere search method. *J. Chem. Phys.* **2008**, 129, 074315. [CrossRef] [PubMed]
- 126. Kang, D.; Dai, J.; Hou, Y.; Yuan, J. Structure and vibrational spectra of small water clusters from first principles simulations. *J. Chem. Phys.* **2010**, *133*, 014302. [CrossRef] [PubMed]
- 127. Bégué, D.; Baraille, I.; Garrain, P.A.; Dargelos, A.; Tassaing, T. Calculation of IR frequencies and intensities in electrical and mechanical anharmonicity approximations: Applications to small water clusters. *J. Chem. Phys.* **2010**, *133*, 034102. [CrossRef] [PubMed]
- 128. Shields, R.M.; Temelso, B.; Archer, K.A.; Morrell, T.E.; Shields, G.C. Accurate Predictions of Water Cluster Formation, $(H_2O)_{n=2-10}$. *J. Phys. Chem. A* **2010**, *114*, 11725–11737. [CrossRef]
- 129. Ramirez, F.; Hadad, C.Z.; Guerra, D.; David, J.; Restrepo, A. Structural Studies of the Water Pentamer. *Chem. Phys. Lett.* **2011**, 507, 229–233. [CrossRef]
- 130. Temelso, B.; Archer, K.A.; Shields, G.C. Benchmark Structures and Binding Energies of Small Water Clusters with Anharmonicity Corrections. *J. Phys. Chem. A* **2011**, *115*, 12034–12046. [CrossRef]
- 131. Temelso, B.; Shields, G.C. The Role of Anharmonicity in Hydrogen-Bonded Systems: The Case of Water Clusters. *J. Chem. Theory Comput.* **2011**, *7*, 2804–2817. [CrossRef]
- 132. Yoo, S.; Xantheas, S.S. Structures, Energetics and Spectroscopic Fingerprints of Water Clusters n = 2-24. In *Handbook of Computational Chemistry*; Leszczynski, J., Ed.; Springer: New York, NY, USA, 2012; Volume 2, pp. 761–792.
- 133. Howard, J.C.; Tschumper, G.S. Wavefunction methods for the accurate characterization of water clusters. *WIREs Comput. Mol. Sci.* **2014**, *4*, 199–224. [CrossRef]
- 134. Howard, J.C.; Tschumper, G.S. Benchmark Structures and Harmonic Vibrational Frequencies Near the CCSD(T) Complete Basis Set Limit for Small Water Clusters: $(H_2O)_{n=2,3,4,5,6}$. *J. Chem. Theory Comput.* **2015**, *11*, 2126–2136. [CrossRef] [PubMed]
- 135. Miliordos, E.; Xantheas, S.S. An accurate and efficient computational protocol for obtaining the complete basis set limits of the binding energies of water clusters at the MP2 and CCSD(T) levels of theory: Application to (H₂O)_m, m = 2–6. 8, 11, 16, and 17. *J. Chem. Phys.* 2015, 142, 234303. [CrossRef] [PubMed]
- 136. Malloum, A.; Fifen, J.J.; Dhaouadi, Z.; Engo, S.G.N.; Conradie, J. Structures, relative stability and binding energies of neutral water clusters, $(H_2O)_{2-30}$. New J. Chem. **2019**, 43, 13020–13037. [CrossRef]
- 137. Møller, C.; Plesset, M.S. Note on an Approximation Treatment for Many-electron Systems. Phys. Rev. 1934, 46, 618–622. [CrossRef]
- 138. Dunning, T.H. Gaussian basis sets for use in correlated molecular calculations. I. The atoms boron through neon and hydrogen. *J. Chem. Phys.* **1989**, *90*, 1007. [CrossRef]
- 139. Kendall, R.A.; Dunning, T.H.; Harrison, R.J. Electron affinities of the first-row atoms revisited. Systematic basis sets and wave functions. *J. Chem. Phys.* **1992**, *96*, 6796–6806. [CrossRef]
- 140. Woon, D.E.; Dunning, T.H. Gaussian basis sets for use in correlated molecular calculations. III. The atoms aluminum through argon. *J. Chem. Phys.* **1993**, *98*, 1358. [CrossRef]
- 141. Bates, D.M.; Smith, J.R.; Janowski, T.; Tschumper, G.S. Development of a 3-body:many-body integrated fragmentation method for weakly bound clusters and application to water clusters (H₂O)_{n=3-10,16,17}. *J. Chem. Phys.* **2011**, 135, 044123. [CrossRef]
- 142. Bates, D.M.; Smith, J.R.; Tschumper, G.S. Efficient and Accurate Methods for the Geometry Optimization of Water Clusters: Application of Analytic Gradients for the Two-Body:Many-Body QM:QM Fragmentation Method to $(H_2O)_n$, n = 3-10. *J. Chem. Theory Comput.* **2011**, 7, 2753–2760. [CrossRef] [PubMed]
- 143. Howard, J.C.; Tschumper, G.S. N-body:Many-body QM:QM vibrational frequencies: Application to small hydrogen-bonded clusters. *J. Chem. Phys.* **2013**, *139*, 184113. [CrossRef] [PubMed]

144. Hopkins, B.W.; Tschumper, G.S. A multicentered approach to integrated QM/QM calculations. Applications to multiply hydrogen-bonded systems. *J. Comput. Chem.* **2003**, 24, 1563–1568. [CrossRef]

- 145. Tschumper, G.S. Multicentered integrated QM:QM methods for weakly bound clusters: An efficient and accurate 2-body:many-body treatment of hydrogen bonding and van der Waals interactions. *Chem. Phys. Lett.* **2006**, 427, 185–191. [CrossRef]
- 146. Elsohly, A.M.; Shaw, C.L.; Guice, M.E.; Smith, B.D.; Tschumper, G.S. Analytic gradients for the multicentered integrated QM:QM method for weakly bound clusters: Efficient and accurate 2-body:many-body geometry optimizations. *Mol. Phys.* 2007, 105, 2777–2782. [CrossRef]
- 147. Tschumper, G.S.; Ellington, T.L.; Johnson, S.N. Chapter Two—Dissociation in Binary Acid/Base Clusters: An Examination of Inconsistencies Introduced Into the Many-Body Expansion by Naíve Fragmentation Schemes. *Annu. Rep. Comput. Chem.* 2017, 13, 93–115. [CrossRef]
- 148. Purvis, G.D., III; Bartlett, R.J. A full coupled-cluster singles and doubles model: The inclusion of disconnected triples. *J. Chem. Phys.* **1982**, *76*, 1910–1918. [CrossRef]
- 149. Stanton, J.F.; Gauss, J.; Cheng, L.; Harding, M.E.; Matthews, D.A.; Szalay, P.G. CFOUR, Coupled-Cluster Techniques for Computational Chemistry, a Quantum-Chemical Program Package. With Contributions from A.A. Auer, R.J. Bartlett, U. Benedikt, C. Berger, D.E. Bernholdt, Y.J. Bomble, O. Christiansen, F. Engel, R. Faber, M. Heckert, O. Heun, M. Hilgenberg, C. Huber, T.-C. Jagau, D. Jonsson, J. Jusélius, T. Kirsch, K. Klein, W.J. Lauderdale, F. Lipparini, T. Metzroth, L.A. Mück, D.P. O'Neill, D.R. Price, E. Prochnow, C. Puzzarini, K. Ruud, F. Schiffmann, W. Schwalbach, C. Simmons, S. Stopkowicz, A. Tajti, J. Vázquez, F. Wang, J.D. Watts and the Integral Packages MOLECULE (J. Almlöf and P.R. Taylor), PROPS (P.R. Taylor), ABACUS (T. Helgaker, H.J. Aa. Jensen, P. Jørgensen, and J. Olsen), and ECP routines by A. V. Mitin and C. van Wüllen. Current Version. Available online: http://www.cfour.de (accessed on 1 December 2023).
- 150. Matthews, D.A.; Cheng, L.; Harding, M.E.; Lipparini, F.; Stopkowicz, S.; Jagau, T.C.; Szalay, P.G.; Gauss, J.; Stanton, J.F. Coupled-cluster techniques for computational chemistry: The CFOUR program package. *J. Chem. Phys.* **2020**, *152*, 214108. [CrossRef]
- 151. Kestner, N.R. He-He Interaction in the SCF-MO Approximation. J. Chem. Phys. 1968, 48, 252–257. [CrossRef]
- 152. Liu, B.; McLean, A.D. Accurate calculation of the attractive interaction of two ground state helium atoms. *J. Chem. Phys.* **1973**, 59, 4557–4558. [CrossRef]
- 153. Jansen, H.B.; Ros, P. Nonempirical molecular orbital calculations on the protonation of carbon monoxide. *Chem. Phys. Lett.* **1969**, 3, 140–143. [CrossRef]
- 154. Boys, S.F.; Bernardi, F. The calculation of small molecular interactions by the differences of separate total energies. Some procedures with reduced errors. *Mol. Phys.* **1970**, *19*, 553–566. [CrossRef]
- 155. Tschumper, G.S. Reliable Electronic Structure Computations for Weak Non-Covalent Interactions in Clusters. In *Reviews in Computational Chemistry*; Lipkowitz, K.B., Cundari, T.R., Eds.; Wiley-VCH, Inc.: Hoboken, NJ, USA, 2008; Volume 26, Chapter 2, pp. 39–90. [CrossRef]
- 156. Jeziorski, B.; Moszynski, R.; Szalewicz, K. Perturbation Theory Approach to Intermolecular Potential Energy Surfaces of van der Waals Complexes. *Chem. Rev.* **1994**, 94, 1887–1930. [CrossRef]
- 157. Hohenstein, E.G.; Sherrill, C.D. Wavefunction methods for noncovalent interactions. *WIREs Comput. Mol. Sci.* **2012**, *2*, 304–326. [CrossRef]
- 158. Szalewicz, K. Symmetry-adapted perturbation theory of intermolecular forces. WIREs Comput. Mol. Sci. 2012, 2, 254–272. [CrossRef]
- 159. Hohenstein, E.G.; Sherrill, C.D. Density fitting of intramonomer correlation effects in symmetry-adapted perturbation theory. *J. Chem. Phys.* **2010**, *133*, 014101. [CrossRef] [PubMed]
- 160. Hohenstein, E.G.; Jaeger, H.M.; Carrell, E.J.; Tschumper, G.S.; Sherrill, C.D. Accurate Interaction Energies for Problematic Dispersion-Bound Complexes: Homogeneous Dimers of NCCN, P₂ and PCCP. *J. Chem. Theory. Comput.* **2011**, 7, 2842–2851. [CrossRef] [PubMed]
- 161. Turney, J.M.; Simmonett, A.C.; Parrish, R.M.; Hohenstein, E.G.; Evangelista, F.A.; Fermann, J.T.; Mintz, B.J.; Burns, L.A.; Wilke, J.J.; Abrams, M.L.; et al. PSI4: An open-source ab initio electronic structure program. *WIREs Comput. Mol. Sci.* **2012**, *2*, 556–565. [CrossRef]
- 162. Smith, D.G.A.; Burns, L.A.; Simmonett, A.C.; Parrish, R.M.; Schieber, M.C.; Galvelis, R.; Kraus, P.; Kruse, H.; Di Remigio, R.; Alenaizan, A.; et al. PSI4 1.4: Open-source software for high-throughput quantum chemistry. *J. Chem. Phys.* **2020**, *152*, 184108. [CrossRef]
- 163. Parrish, R.M.; Sherrill, C.D. Tractability gains in symmetry-adapted perturbation theory including coupled double excitations: CCD+ST(CCD) dispersion with natural orbital truncations. *J. Chem. Phys.* **2013**, *139*, 174102. [CrossRef]

Disclaimer/Publisher's Note: The statements, opinions and data contained in all publications are solely those of the individual author(s) and contributor(s) and not of MDPI and/or the editor(s). MDPI and/or the editor(s) disclaim responsibility for any injury to people or property resulting from any ideas, methods, instructions or products referred to in the content.